Imaging Characteristics of the Axicon Imaging System

Zhongsheng Zhai[1], Qinghua Lv[2,3], Xuanze Wang[1], Liangen Yang[1], Zhongbao Xu[1] and He Tao[1]

[1] School of Mechanics and Engineering, Hubei University of Technology, Lizhi Road, Wuhan, Hubei, China
[2] Hubei Collaborative Innovation Center for High-efficient Utilization of Solar Energy,
Hubei University of Technology, Lizhi Road, Wuhan, Hubei, China
[3] School of Science, Hubei University of Technology, Lizhi Road, Wuhan, Hubei, China

Keywords: Depth of Field, Non-diffracting Beams, Axicon, Imaging Characteristics.

Abstract: The depth of an image system can be extended by an axicon which can generate line focus. According to physical optical theory, the diffracting patterns of the defocus point spread function (PSF) for the imaging system with axicon are analyzed through the generalize pupil function. The expressions of the PSF for the imaging system illuminated by white light are described as the superposition of the intensities in individual monochromatic patterns. Experimental results show that the central portion contains the most energy of the diffraction pattern from the PSF produced by the white light, and the contrast of secondary outside circular rings decreased rapidly. Furthermore，the central spot radius varied slowly with the increase of defocus parameter, and the depth of field of the imaging system is effectively extended with a shortcoming that the images need further processing.

1 INTRODUCTION

In 1987, the team of J. Durnin found the solution of the Maxwell's wave equation, which was given as zero-order Bessel function forms, and first put forward the concept of nondiffracting beams (Durnin, 1987). Nondiffracting beams which has characteristics that the size of central spot and shape does not change significantly over a propagation distance. In 1992, G. Scott and other researchers used the axicon to generate nondiffracting beams (Scott and McArdie, 1992).

The 'axicon', first introduced by McLeod in 1954, can form an extended focal segment which has the zero-order Bessel distribution, and it can also generate annular beams in the far region. (McLeod, 1954). Axicons have been incorporated in numerous applications. Zhai using the axicon, simulated by a spatial light modulator to to improved the efficiency of laser processing (Zhai and Kuang, 2014). Guillaume Druart demonstrated the diffractive axcion has image-zooming capability, and they realized a x2 linear system (Druart et al., 2008). Zeng et al. used a refractive axicon to transform an input Gaussian laser beam into a collimated annular beam, which refer to as optical trepanning. (Zeng et al., 2006).

In recent years the ability of annular linear axicons for extending the depth of field of imaging system has proposed by some researchers (Mikula et al., 2005). They fixed the distance between the input object and the diffractive elements, and obtained output images in different output planes behind the axicon. In an early publication (Zhai and Zhao, 2007), we have derived the diffraction patterns of an axicon illuminated by a red high brightness LED, and the patterns were looked as the PSFs of the axicon imaging system. However, the expressions of the PSFs were calculated by the point light source in different positions，not by the defocus aberration.

The aim of this paper is to analyze the imaging principle of axicon, and to analyze the relationship between the PSF and the defocus parameter. Imaging results proved that the axicon can extend the depth of field. The images created by this system can be observed in real time, but they exhibit a very poor contrast. For getting clearer images, digital processing method is required.

2 THEORIES

2.1 Defocus Aberration

It is well known that defocus aberration manifests itself by a quadratic phase at the imaging system pupil, i.e.

$$G(u,v,\varphi) = \exp[i\varphi(u^2 + v^2)] \tag{1}$$

where (u, v) are the normalized coordinates of the pupil plane, and the defocus parameter φ is defined by the following expression (Eliezer et al., 2008):

$$\varphi = \frac{2\pi}{\lambda} W_{20} = \frac{\pi d^2}{\lambda}(\frac{1}{l'} - \frac{1}{l} - \frac{1}{f}) \tag{2}$$

where W_{20} is Hopkins defocus factor, d is the pupil radius, λ is the wavelength, f, l and l' are the lens focal length, the distances from the object and the image to the lens respectively.

Obviously, when imaging condition is fulfilled:

$$\frac{1}{l'} - \frac{1}{l} - \frac{1}{f} = 0 \tag{3}$$

From equation 2, we can observe that the defocus parameter φ equals zero. In the large DOF imaging system, when a focus aberration occurs, as shown in figure 1, the wavefront is deformed and it can use the generalize pupil function to describe the defocus error. The defocus factor is given as:

$$W_{20} = \frac{1}{2}(\frac{1}{z_a} - \frac{1}{z_l}) \cdot r^2 \tag{4}$$

where r is the radius of the pupil. z_l is the distance from the ideal image plane to the lens, and z_a is the distance between the lens and the defocus image plane. In the common imaging system, the defocus factor is changed with the increase of z_a.
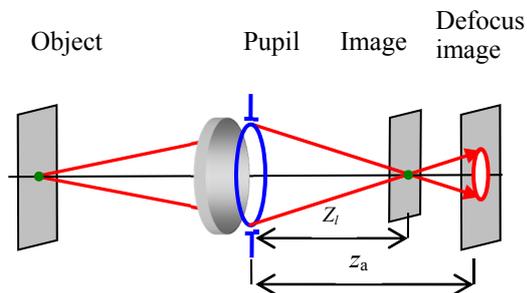

Figure 1: Scheme of defocus system.

2.2 Imaging System Design

An imaging system was arranged as shown in figure 2. It mainly includes a light source, battery of lens, an axicon, a CCD detector and a computer. The axicon is placed at the back of lens, and a CCD camera is used to capture intermediate images when the object moves within a specified region before the lens. The object is illuminated with incoherent light. The quality of the intermediate images is so poor that an image processing portion is needed. For better considering the depth of field, in the designed imaging system, the distances between the lens, axicon and CCD camera are fixed. It requires post-processing steps in order to achieve a high quality image, so it is a two step imaging system.
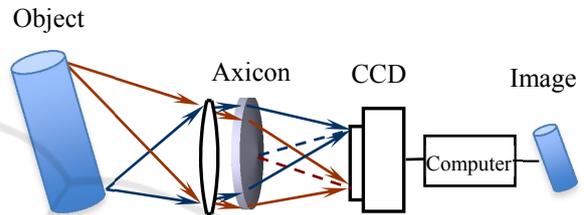

Figure 2: Schematic diagram of non- diffractive beam imaging system.

2.3 PSF of Defocus

Consider a thin axicon with a transmittance function given by

$$t(r) = \begin{cases} \exp\left[\dfrac{-ik(n-1)\theta D}{2}\sqrt{u^2+v^2}\right] & \sqrt{u^2+v^2} \leq 1 \\ 0 & \sqrt{u^2+v^2} > 1 \end{cases} \tag{5}$$

where u, v are the normalized pupil coordinates, n is the refractive index, D is the diameter of the axicon, k is the wave number $2\pi/\lambda$, and θ is refracting angle.

After putting the axicon in the pupil of the imaging system, when aberrations are introduced, the generalized pupil function may be described as

$$Q(u,v,\varphi) = t(u,v)G(u,v,\varphi)$$
$$= \exp[\frac{-ik(n-1)\theta D}{2}\sqrt{u^2+v^2}]\exp[i\varphi(u^2+v^2)] \tag{6}$$

where φ is the defocus parameter.

According to the theory of Fourier optics, in the diffraction-limited imaging system, the point spread function is the Fraunhofer diffraction pattern of pupil function. Therefore, we can obtain the PSF of the system with the axicon as:

$$h(x,y,\varphi) = \frac{A}{\lambda z_i} \iint Q(u,v,\varphi) \exp\{i\frac{2\pi}{\lambda z_i}[xu+yv]\}dudv$$

$$= \iint \exp[\frac{-ik(n-1)\theta D}{2}\sqrt{u^2+v^2}]\exp[i\varphi(u^2+v^2)] \qquad (7)$$

$$\cdot \exp\{i\frac{2\pi}{\lambda z_i}[xu+yv]\}dudv$$

where A is the amplitude of the incident beam, Z_i is the distance from the axicon to the image plane.

The optical system is circular symmetry, and for the sake of simplicity, we make a transformation to polar coordinates in both the (u, v) and the (x, y) planes as follows:

$$
\begin{aligned}
\rho &= \sqrt{u^2+v^2} \\
\beta &= \arctan(\frac{v}{u}) \\
u &= \rho\cos\beta, \ v = \rho\sin\beta \\
\rho_1 &= \sqrt{x^2+y^2} \\
\gamma &= \arctan(\frac{y}{x}) \\
x &= \rho_1\cos\gamma, \ y = \rho_1\sin\gamma
\end{aligned}
\qquad (8)
$$

Applying the coordinate transforms, the PSF can be written as

$$h(\rho_1,\varphi) = \int \rho \exp[\frac{-ik(n-1)\theta D}{2}\rho + i\varphi\rho^2]d\rho$$

$$\cdot \int_0^{2\pi} \exp[-i\frac{2\pi}{\lambda z_i}\rho\rho_1\cos(\beta-\gamma)]d\beta \qquad (9)$$

Taking into account the circular symmetry of the second integral in Eq (9), we use the Bessel function identity

$$\int_0^{2\pi} \exp[ia\cos(\beta-\gamma)]d\beta = 2\pi J_0(a) \qquad (10)$$

where J_0 is a Bessel function of the first kind, zero order. Substituting (10) in Eq.(9), we can obtain

$$h(\rho_1,\varphi) = 2\pi \int \rho J_0(\frac{2\pi}{\lambda z_i}\rho\rho_1)$$

$$\cdot \exp[\frac{-ik(n-1)\theta D}{2}\rho + i\varphi\rho^2]d\rho \qquad (11)$$

With the stationary phase method (Goodman, 1996), Eq. (11) can be approximated by following:

$$h(\rho_1,\varphi) \approx 2\pi\sqrt{\frac{\pi}{|\varphi|}}\rho_s J_0(\frac{2\pi}{\lambda z_i}\rho_s\rho_1)$$

$$\cdot \exp[\frac{-ik(n-1)\theta D}{2}\rho_s + i\varphi\rho_s^2] \qquad (12)$$

where ρ_s is the stationary point,

$$\rho_s = \frac{k(n-1)\theta D}{4\varphi} \qquad (13)$$

In an incoherent imaging system, the intensity of point spread function can be given by

$$h_I(x,y,\varphi) = |h(x,y,\varphi)|^2 = |F\{Q(\rho,\varphi)\}|^2 \qquad (14)$$

For the sake of simplicity, 1-D analysis of Eq.(14) is performed as:

$$h_I(\rho_1,\varphi) \approx \frac{4\pi^3}{|\varphi|}\rho_s J_0^2(\frac{2\pi}{\lambda z_i}\rho_s\rho_1)$$

$$= \frac{4\pi^3}{|kW_{20}|}\rho_s J_0^2(\frac{k(n-1)\theta D}{z_i W_{20}}\rho_1) \qquad (15)$$

Note that Eq.(15) is the expression of the PSF of the axicon imaging system under monochromatic light. If the light source is polychromatic light or white light, the PSFs for the these source are different from Eq.(15). The white light can be represented by a combination of mutually incoherent monochromatic components extending over a range of frequencies. Each component produces a diffraction pattern as described above, and the total intensity is everywhere the sum of the intensities in these monochromatic patterns. If the wavelength bandwidth of the light source is $\lambda \in [\lambda_{beg}, \lambda_{end}]$, the PSF of imaging system with axicon illuminated with white light can be expressed as

$$h_I(\rho_1,\varphi) = \int_{\lambda_{beg}}^{\lambda_{end}} \frac{4\pi^3}{|\varphi|}\rho_s J_0^2(\frac{k(n-1)\theta D}{z_i W_{20}}\rho_1)d\lambda \quad (16)$$

3 SIMULATION AND EXPERIMENT

To demonstrate the above theoretical analysis, we have carried out numerical simulations and experiments. Numerical simulations for the PSFs at different defocus aberration conditions $\varphi = 0.5\pi, \pi, 2\pi, 4\pi$, were done by use of Eq. (16), as shown in figure 3.

Some parameters were given by $\theta = 0.05$, $n = 1.5$, $z = 120$mm, $f = 120$mm, $D = 10$mm and $\lambda \in [380, 780]$ nm. From figure 3, it follows that the central spot radius varied with the change of defocus parameter φ.

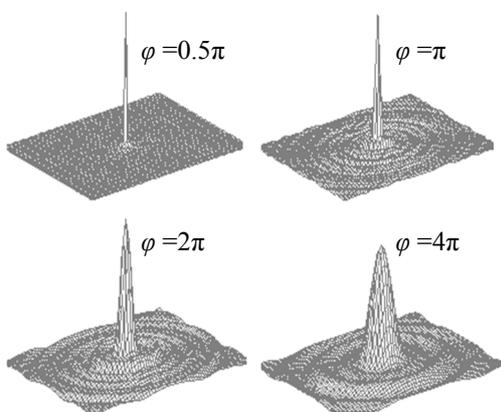Figure 3: Simulation of PSFs for different φ.

An experimental imaging system was constructed based on figure 2, and some parameters of this imaging system are the refractive index of the axicon $n = 1.5$, the refracting angle of the axicon $\theta = 0.01$rad. Figure 4 gives the experiment result of the normalized PSFs for the system under incoherent illumination in case of $l = 160$, 210, 260, 310mm. Obviously, the central portion contains the most energy of the diffraction pattern from the PSF produced by the white light, and the contrast of secondary outside circular rings decreased rapidly. Therefore, the imaging characteristics of the system with the axicon are mainly determined by the central spot.
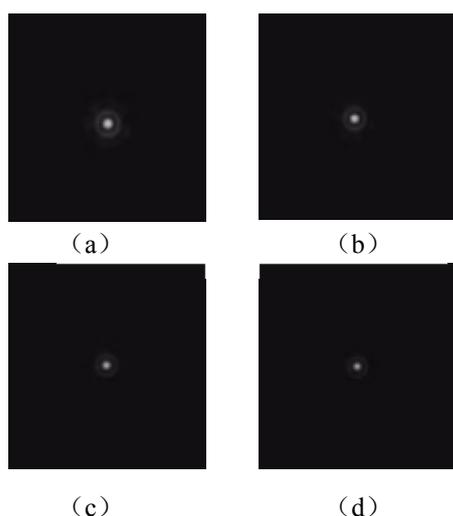

Figure 4: Experiment results of the PSFs for different l. (a) 160mm, (b) 210mm, (c) 260mm, (d) 310mm.
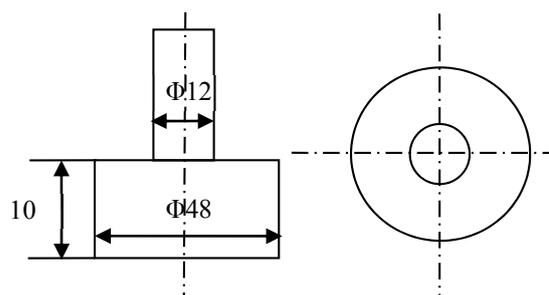
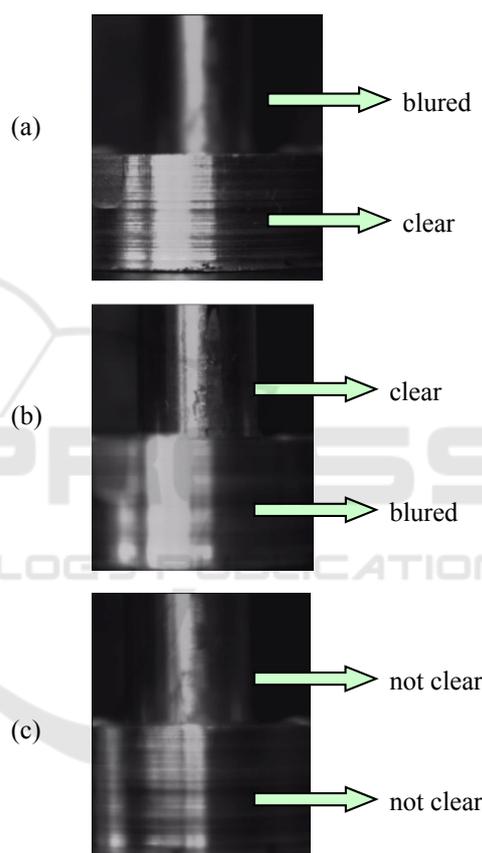

Figure 5: Structural diagram of a candlestick.

Figure 6: Imaging results by the system (a) (b) without the axicon, (c) with the axicon.

An imaging experiment for a candlestick with two different diameter parts was exhibited using the same system. Figure 5 presents the structure diagram. The images in figure 6(a) and 6(b) were taken by the standard imaging system without the axicon, and the image in figure 6(c) was acquired in the case of the system with the axicon. From figure 6(a) and 6(b), it is obvious that only one part of the candlestick is clear which is in the focus plane, and the other part is blurring for the reason of defocus.

In figure 6(c), we also can observe that even the

images of the both parts of the candlestick are not as clear as the images in focus plane, but they are more clear than those in the out of focus place. Therefore the image acquired by the imaging system with the axicon is insensitive to defocus, and the depth of field of the imaging system is effectively extended. However, it has a shortcoming that the images have low contrast and low resolution. The quality of the intermediate images is so poor that an image processing portion is needed.

4 CONCLUSIONS

We have investigated the imaging feature of the axicon for extending depth of field. The diffraction intensity distribution of PSFs of the imaging system illuminated with monochromatic and white light are clearly derived based on the generalize pupil function. The experimental results proved that the PSF for white light could be obtained by the superposition of the intensities in individual monochromatic patterns, and imaging results showed that the axion can extend the depth of the field with unclear images which need further processing.

REFERENCES

J. Durnin, 1987. *Exact solutions for Nondiffracting Beams*, Physical Review Letters. 58, 1479-1501 .

G. Scott, N. McArdie, 1992. *Efficient generation of nearly diffraction-free beams using an axicon*. Optical Engineering 31(12), 2640-2643.

H. J. Mcleod, 1954. *The axicon: a new type of optical element,* J. Opt. Soc. Am. 44, 592-597.

Z. Zhai, Z. Kuang, et al. 2014. *Synchronization control for Ultrafast laser parallel microdrilling system* SPIE 9271.

G. Druart, J. Taboury,et al, 2008. *Demonstration of image-zooming capability for diffractive axicons*. Optics Letter, 33, 366-368.

D. Zeng, W. P. Latham, A. Kar, 2006. *Characteristic analysis of a refractive axicon system for optical trepanning*, Optical Engineering. 45(9), 094302 .

G. Mikula, A. Kolodziejczyk, M, Makowski. 2005. *Diffractive elements for imaging with extended depth of focus*, Optical Engneering, 44, 058001-1-7.

Z. Zhai, B. Zhao, 2007. *Diffraction Intensity distribution of an axicon illuminated by polychromatic light*. Journal of Optics A: Pure and Applied Optics, 9(10): 862-867.

E. B. Eliezer, N. Konforti, et al, 2008. *An optimal binary amplitude-phase mask for hybrid imaging systems that exhibit high resolution and extended depth of field*. Optics Express,16(25), 20540-61.

J. W. Goodman, 1996. *Introduction to Fourier Optics*, McGraw-Hill, New York,.